Multiplexed imaging of Barrett's neoplasia using targeted fluorescent heptapeptides and multimodal scanning fiber endoscope: a phase 1, open-label, proof-of-concept study

Jing Chen,[1] Yang Jiang,[2] Tse-Shao Chang,[3] Bishnu Joshi,[1] Juan Zhou,[1] Joel H Rubenstein,[1] Erik J Wamsteker,[1] Richard S Kwon,[1] Henry Appelman,[4] David G Beer,[5] Danielle K Turgeon,[1] Eric J Seibel,[2] Thomas D Wang[1,3,7]

Supplementary methods

Fluorescently-labeled peptides

QRHKPRE was labeled with Cy5 via a GGGSK linker to prevent steric hindrance, hereafter QRH*-Cy5. This sequence was selected using phage display methods for specific binding to EGFR. KSPNPRF was labeled with IRDye800 via a GGGSC linker, hereafter KSP*-IRDye800. This sequence was identified using a structural model for specific binding to ErbB2. The fluorophores used were chosen to minimize spectral overlap between absorbance and emission. QRH*-Cy5 and KSP*-IRDye800 were synthesized using current good manufacturing practices (cGMP) methods. Peptide stability was monitored by visual appearance, purity (HPLC), and molecular weight over the duration of the study.

Pharmacology/toxicology study

A rigorous pharmacology/toxicology study was performed in animals (MPI Research) for each peptide to provide pre-clinical evidence for safety. A total of 24 male and 24 female rats (CD®[Crl:CD®(SD)] (Charles River) were used in each study. At 8 weeks of age, the animals were randomly assigned to 4 groups, including 3 treatment and 1 control. Dose levels of 0.0086, 0.026, and 0.86 mg/kg were used for QRH*-Cy5, and 0.186, 0.32, and 1.08 mg/kg were used for KSP*-

Chen J, *et al. Gut* 2021; 70:1010–1013. doi: 10.1136/gutjnl-2020-322945

IRDye800. The control group received 10 mL/kg of PBS as vehicle. The vehicle and test articles were administered by single dose oral gavage. Clinical signs, including morbidity, mortality, and injury, were monitored twice daily. Laboratory tests and necropsy were evaluated in 3 animals/sex/dose on days 2 and 15.

Phase 1 safety study

A first-in-human study was performed to establish clinical evidence of safety for each peptide. An Investigational New Drug (IND) application (sponsor DKT) was prepared, and submitted for review to the US Food and Drug Administration (FDA). The chemistry, manufacturing, and control (CMC) document for cGMP peptide synthesis, animal pharmacology/toxicology results, and study protocol were included. The study protocols were reviewed and approved by the Institutional Review Board (IRB) at Michigan Medicine. These studies, including NCT02574858 (QRH*-Cy5) and NCT03161418 (KSP*-IRDye800), were registered online at ClinicalTrials.gov. A total of n = 25 subjects was recruited for each study. All enrolled patients provided written informed consent. A dose escalation study was performed. The first n = 3 subjects were administered 0.5 mg of peptide reconstituted in 5 mL of normal saline (0.9%) per oral. Laboratory tests, including complete blood count (CBC), chemistries, liver function tests (LFT), and urinalysis (UA), were collected before and ~24 hours after peptide administration. An EKG was performed, and vital signs were monitored. After finding no peptide-related abnormalities, the remaining n = 22 subjects received the higher dose of 1.2 mg. No images were collected during the safety study.

Chen J, *et al. Gut* 2021; 70:1010–1013. doi: 10.1136/gutjnl-2020-322945

Multiplexed imaging instrument

A multi-modal scanning fiber endoscope (mmSFE) was designed to collect fluorescence and reflectance concurrently. A custom fiber-coupled multi-laser system (SpectraTEC, Blue Sky Research) provides illumination at λ_{ex} = 638 and 785 nm concurrently through a single mode fiber (SMF) to excite QRH*-Cy5 and KSP*-IRDye800, respectively. A 0.4 mm diameter metal coated piezo tube actuator (Nagamine) generates a spiral scan pattern at an average maximum deflection angle of ~70°. Large core (500 μm diameter) multi-mode fibers (MMF) with high numerical aperture (NA = 0.6, Mitsubishi Rayon) are arranged around the instrument periphery to maximize light collection. The diameter and rigid length of the distal tip was compact to pass forward easily through the working channel of a standard upper endoscope.

The optics used to separate and collect fluorescence from each peptide was contained within the base station (VerAvanti). A notch filter (NF, #NF03-785E-25, Semrock) was used to attenuate the excitation beam at λ = 785 nm. Reflectance at λ = 647 nm was deflected by a dichroic beam splitter (BS_1, #FF652-Di02, Semrock) to a multi-pixel photon counter ($MPPC_1$, SiPM, Hamamatsu) for detection. Fluorescence from QRH*-Cy5 was deflected by a second beam splitter (BS_2, #Di02-R785, Semrock) centered at λ = 785 nm through a bandpass filter (BPF, FF01-697/58, Semrock) that transmits between 668-726 nm for detection by $MPPC_2$. Fluorescence from KSP*-IRDye800 passes through BS_2 and long pass filter (LPF, #BLP01-785R, Semrock) with cutoff at λ = 805 nm and is detected by $MPPC_3$. Kinematic filter cubes (DFM1/M, ThorLabs) were used to mount and align the optics.

In vivo imaging

Consecutive patients referred to Michigan Medicine for either evaluation or therapy of Barrett's neoplasia were recruited. Inclusion criteria included: 1) history of Barrett's neoplasia, 2)

Chen J, *et al. Gut* 2021; 70:1010–1013. doi: 10.1136/gutjnl-2020-322945

medically able to tolerate upper endoscopy, and 3) age over 18. Exclusion criteria included: 1) history of esophagectomy and 2) on active chemotherapy or radiation protocol. The multiplexed imaging study was approved by the IRB, and was registered online at ClinicalTrials.gov (NCT03589443). All authors had access to the study data, contributed to this manuscript's writing and review, and approved the final manuscript.

The QRH*-Cy5 and KSP*-IRDye800 were reconstituted in 5 mL of normal saline separately, and topically administered in the distal esophagus using a standard spray catheter (PW-5V-1, Olympus Medical Systems Corp) passed through the instrument channel of the endoscope. Separate channels were used to record fluorescence images from QRH*-Cy5 and KSP*-IRDye800 and from reflectance at $\lambda = 638$ nm. The conventional white light illumination was shut off during collection of fluorescence images to prevent interference. Tissue specimens were collected with either biopsy or EMR from suspicious regions. The most advanced histological classification for each subject is shown, Table 1.

Image analysis

Video streams with >30 consecutive fluorescence images (1 sec) having negligible artifacts, including debris, bubbles, pooling, and interference from conventional white light illumination, were extracted from the original recordings. Single frames from the target regions with high contrast and minimum motion blur and distortion were selected for intensity quantification. The frames were separated into two fluorescence channels and a co-registered reflectance image. Target/background (T/B) ratios were calculated for each fluorescence image as follows. A 5×5 Gaussian filter was used first to smooth the image. Fluorescence regions with high intensity were segmented using the Chan-Vese algorithm,[1] where an active contour model was

evolved iteratively to minimize the energy function, Eq. 1, defined by the weighted sum of the 1) boundary length, 2) area, and variance of intensity 3) inside and 4) outside of the segmented region.

$$F(\varphi) = \mu\int_{\Omega}|\nabla H(\varphi)|\,dx + v\int_{\Omega}H(\varphi)dx + \lambda_1\int_{\Omega}|I-c_1|^2\,H(\varphi)dx + \lambda_2\int_{\Omega}|I-c_2|^2\,(1-H(\varphi))dx, \quad (1)$$

where H is the Heavyside function, ϕ is the level set function, I is the segmented image, and Ω is the image domain. Coefficients c_1 and c_2 are the average intensities inside and outside of the segmented region, respectively. The regulation parameters μ, ν, λ_1, λ_2 represent the energy functions, where μ and ν penalizes the total boundary length and area, respectively, of the segmented region. The intensity variance inside and outside of the segmented regions is represented by λ_1 and λ_2, respectively.

After image segmentation, a series of standard morphology operations, including erosion and dilation, were implemented using OpenCV library.[2] Erosion was performed to smooth the target region by removing isolated noise <10 pixels. Dilation was done to enlarge the boundaries of the target region and generate an adjacent 30 pixel-wide background. T/B ratios were calculated from the mean intensities each region. The T/B ratios were used to classify each patient as being either positive (HGD/EAC) or negative (SQ/NDBE/LGD) based on the highest grade of pathology found. Different methods were investigated to classify the data, including the 1,2) T/B ratios from each fluorescence channel separately, 3) maximum T/B ratio, 4) logistic regression with L2 regularization which prevents overfitting of the model, and 5) support vector machine (SVM), which constructs a hyperplane. A leave-one-out cross-validation (LOOCV) was performed to identify the best method.[3] For each round, the T/B ratios from n = 21 subjects were used as a training set to determine the discriminant function used to assign a score to the left-out subject. For methods 1-3, the maximum Youden index of the receiver operating characteristic (ROC) curve

Chen J, *et al. Gut* 2021; 70:1010–1013. doi: 10.1136/gutjnl-2020-322945

was used to select the optimal cutoff threshold for HGD/EAC, which maximizes the vertical distance between the ROC curve and the diagonal line.[4] Normally, the Youden index is defined as sensitivity +, specificity – 1.

For logistic regression and SVM, a nested cross validation was performed to select the hyperparameters for each model, including C-values (inverse of L2 regularization strength) for logistic regression, γ-values (kernel coefficient), and C-values for SVM with a radial basis function (RBF) kernel. A repeated stratified 9-fold cross-validation in the inner loop was used to select the hyperparameters that provided the maximal classification accuracy for the 21 samples. The model was refit with these optimal values using n = 21 data points, and then the result left out in the outer loop was evaluated. The average classification accuracy of each method from LOOCV was compared. The sensitivity, specificity, and area-under-the-curve (AUC) for the ROC curve using LOOCV was computed and compared for logistic regression and SVM. The optimal model was then retrained using all data. The performance of multiplexed detection using the trained optimal model was then compared with that for use of either QRH*-Cy5 or KSP*-IRDye800 alone with an average ROC curve taken from 1000 bootstrap samples. The analysis was implemented using Python using scikit-learn library.[5]

Reference

1. Jiang, Y., Gong, Y., Rubenstein, J. H., Wang, T. D. & Seibel, E. J. Toward real-time quantification of fluorescence molecular probes using target/background ratio for guiding biopsy and endoscopic therapy of esophageal neoplasia. *J. Med. Imaging* **4**, 024502 (2017).
2. Bradski, G. & Kaehler, A. in *learning OpenCV* (O'Reilly media, 2008).
3. Kohavi, R. A study of cross-validation and bootstrap for accuracy estimation and model selection. IJCAI. **14**, 1137-1145 (1995).
4. Hajian-Tilaki, K. Receiver operating characteristic (ROC) curve analysis for medical diagnostic test evaluation. *Caspian J. Intern. Med.* **4**, 627 (2013).
5. Pedregosa, F. et al. Scikit-learn: machine learning in python, *J. Mach. Learn. Res.* **12**, 2825-2830 (2011).

Supplementary Tables

Supplementary Table 1 – GMP synthesis of QRH*-Cy5

Attributes	Test Methods	Specifications	Results
Appearance	visual	blue powder	blue powder
Purity (%)	HPLC	≥95.0%	96.0%
		Glx 1.70-2.30	Glx 2.01
		Arg 1.70-2.30	Arg 2.05
		His 0.85-1.15	His 0.98
Amino acid analysis	UPLC	Pro 0.85-1.15	Pro 0.99
		Gly 2.55-3.45	Gly 2.97
		Lys 1.70-2.30	Lys 2.01
		Ser report	Ser 0.83
Peptide content	UPLC	report	70.3%
Primary counter ion	HPLC	TFA	TFA
TFA content	HPLC	report	18.5%
Water Content (%w/w)	Karl Fisher	report	5.1%
Endotoxin	SOP	report	<1 EU/mg
Bioburden	SOP	report	<1 CFU/mg
Molecular weight	ESI-MS	1973.3±1.0	1973.0

Note: The final bulk material consisted of Gln^{1}-Arg^{2}-His^{3}-Lys^{4}-Pro^{5}-Arg^{6}-Glu^{7}-Gly^{8}-Gly^{9}-Gly^{10}-Ser^{11}-Lys^{12}(Cy^{5})-NH_2 with the formula: $C_{86}H_{129}N_{26}NaO_{23}S_2$. Attributes of QRH*-Cy5 are documented on a certificate of analysis (COA) by cGMP vendor. Key: CFU, colony-forming unit; ESI-MS, electrospray ionization mass spectrometry; EU, endotoxin unit; HPLC, high performance liquid chromatography; SOP, standard operating procedure; TFA, trifluoroacetic acid; UPLC, ultra-performance liquid chromatography.

Supplementary Table 2 – GMP synthesis of KSP*-IRDye800

Attributes	Test Methods	Specifications	Results
Appearance	visual	dark green powder	dark green powder
Purity (%)	HPLC	≥95.0%	98.8%
Amino acid analysis	UPLC	Arg 0.85-1.15	Arg 0.99
		Gly 2.55-3.45	Gly 2.96
		Asn 0.85-1.15	Asn 1.05
		Pro 1.70-2.30	Pro 1.99
		Lys 0.85-1.15	Lys 1.00
		Phe 0.85-1.15	Phe 1.02
		Ser report	Ser 1.52
		Cys report	Cys 0.00
Peptide content	UPLC	report	91.9%
Primary counter ion	HPLC	acetate	acetate
Acetic acid content	HPLC	report	0.6%
Water content (%w/w)	Karl Fisher	report	9.0%
Endotoxin	SOP	report	<1 EU/mg
Bioburden	SOP	report	<1 CFU/mg
Molecular weight	ESI-MS	2397.6±1.0	2397.6

Note: The final bulk material consisted of Lys^{1}-Ser^{2}-Pro^{3}-Asn^{4}-Pro^{5}-Arg^{6}-Phe^{7}-Gly^{8}-Gly^{9}-Gly^{10}-Ser^{11}-Cys^{12}(IRDye800) with the formula: $C_{102}H_{136}N_{21}Na_3O_{32}S_5$. Attributes of KSP*-IRDye800 are documented on a certificate of analysis (COA) by cGMP vendor. Key: CFU, colony-forming unit; ESI-MS, electrospray ionization mass spectrometry; EU, endotoxin unit; HPLC, high performance liquid chromatography; SOP, standard operating procedure; UPLC, ultra-performance liquid chromatography.

Chen J, *et al. Gut* 2021; 70:1010–1013. doi: 10.1136/gutjnl-2020-322945

Supplementary Table 3 – Stability of QRH*-Cy5

Time (Months)	0	6	12	18	24	30	36
Appearance	blue	blue	blue	blue	blue	blue	blue
Purity	96.0%	96.2%	96.3%	97.1%	96.2%	96.4%	96.1%
Molecular Weight	1974.3	N/A	1972.6	N/A	1973.7	N/A	1973.3

Note: Lyophilized peptides are stored at -20ºC under dry conditions and are protected from light in an amber tube. Purity was analyzed by high performance liquid chromatography (HPLC). Molecular weight was measured using Q-TOF mass spectrometer.

Chen J, *et al. Gut* 2021; 70:1010–1013. doi: 10.1136/gutjnl-2020-322945

Supplementary Table 4 – Stability of KSP*-IRDye800

Time (Months)	0	6	12	18	24	30	36
Appearance	dark green	dark green	dark green	dark green	dark green	dark green	dark green
Purity (HPLC)	98.8%	98.8%	98.7%	98.9%	98.9%	98.7%	98.9%
Molecular Weight	2397.6	N/A	2397.5	N/A	2397.6	N/A	2397.6

Note: Lyophilized peptides are stored at -20ºC under dry conditions and are protected from light in an amber tube. Purity was analyzed by high performance liquid chromatography (HPLC). Molecular weight was measured using Q-TOF mass spectrometer.

Chen J, *et al. Gut* 2021; 70:1010–1013. doi: 10.1136/gutjnl-2020-322945

Supplementary Table 5 – Animal pharmacology/toxicology study of QRH*-Cy5

No	Dose level (mg/kg)	Volume (mL/kg)	M	F	Observe	Clinical signs	Blood tests (days 2 and 15)	Necropsy (days 2 and 15)	Urinalysis
1	0	10	6	6	NAD	NAD	NAD	NAD	NAD
2	0.0086	1	6	6	NAD	NAD	NAD	NAD	NAD
3	0.026	1	6	6	NAD	NAD	NAD	NAD	NAD
4	0.86	10	6	6	NAD	NAD	NAD	NAD	NAD

Observe	Clinical signs	Blood tests			Necropsy	Urinalysis
		Hematology	Clinical chemistries	Coagulation factors		
Morbidity, mortality, injury, body weights, food and water consumption	Skin, fur, eyes, ears, nose, oral cavity, thorax, abdomen, external genitalia, limbs and feet; respiratory and circulatory effects; autonomic effects (salivation); nervous system effects (tremors, convulsions, reactivity to handling and unusual behavior)	Leukocyte count (total and absolute differential), erythrocyte count, hemoglobin, hematocrit, mean corpuscular hemoglobin (volume and concentration), platelet count, absolute reticulocytes, blood cell morphology	Alkaline phosphatase, total bilirubin, aspartate aminotransferase, alanine aminotransferase, urea nitrogen, creatinine, total protein, albumin, globulin and A/G (albumin/globulin) ratio, glucose, total cholesterol, triglycerides, sodium, potassium, chloride, calcium, phosphorus	Prothrombin time, activated partial thromboplastin time, fibrinogen	Macroscopic exam for external abnormalities; recording of organ weights; microscopic exam of bone with bone marrow (femur, sternum), brain (cerebrum, midbrain, cerebellum, medulla, pons), esophagus, heart, kidney, liver, lung with bronchi, lymph nodes (mesenteric), small intestine (duodenum, ileum, jejunum), spleen, stomach (glandular, nonglandular) and thymus.	Volume, color and appearance, specific gravity, pH, protein, glucose, bilirubin, ketones, blood, urobilinogen, microscopy of centrifuged sediment

Notes: Acute test article-related effects in 7-week-old CD[Crl:CD(SD)] rats (n = 48) after oral gavage administration of cGMP-synthesized QRH*-Cy5 are shown. Phosphate-buffered saline (pH = 7.4) was used as vehicle. Animal were monitored at specific time points over the course of 15 days after peptide administration. For necropsy, 3 animals/sex/group were euthanized on days 2 and 15. NAD – No abnormalities detected.

Chen J, *et al. Gut* 2021; 70:1010–1013. doi: 10.1136/gutjnl-2020-322945

Supplementary Table 6 – Animal pharmacology/toxicology study of KSP*-IRDye800

No	Dose level (mg/kg)	Volume (mL/kg)	M	F	Observe	Clinical signs	Blood tests (days 2 and 15)	Necropsy (days 2 and 15)	Urinalysis
1	0	10	6	6	NAD	NAD	NAD	NAD	NAD
2	0.186	10	6	6	NAD	NAD	NAD	NAD	NAD
3	0.32	10	6	6	NAD	NAD	NAD	NAD	NAD
4	1.08	10	6	6	NAD	NAD	NAD	NAD	NAD

Observe	Clinical signs	Blood tests			Necropsy	Urinalysis
		Hematology	Clinical chemistries	Coagulation factors		
Morbidity, mortality, injury, body weights, food and water consumption	Skin, fur, eyes, ears, nose, oral cavity, thorax, abdomen, external genitalia, limbs and feet; respiratory and circulatory effects; autonomic effects (salivation); nervous system effects (tremors, convulsions, reactivity to handling and unusual behavior)	Leukocyte count (total and absolute differential), erythrocyte count, hemoglobin, hematocrit, mean corpuscular hemoglobin (volume and concentration), platelet count, absolute reticulocytes, blood cell morphology	Alkaline phosphatase, total bilirubin, aspartate aminotransferase, alanine aminotransferase, urea nitrogen, creatinine, total protein, albumin, globulin and A/G (albumin/globulin) ratio, glucose, total cholesterol, triglycerides, sodium, potassium, chloride, calcium, phosphorus	Prothrombin time, activated partial thromboplastin time, fibrinogen	Macroscopic exam for external abnormalities; recording of organ weights; microscopic exam of bone with bone marrow (femur, sternum), brain (cerebrum, midbrain, cerebellum, medulla, pons), esophagus, heart, kidney, liver, lung with bronchi, lymph nodes (mesenteric), small intestine (duodenum, ileum, jejunum), spleen, stomach (glandular, nonglandular) and thymus.	Volume, color and appearance, specific gravity, pH, protein, glucose, bilirubin, ketones, blood, urobilinogen, microscopy of centrifuged sediment

Notes: Acute test article-related effects in 7-week-old CD[Crl:CD(SD)] rats (n = 48) after oral gavage administration of cGMP-synthesized KSP*-IRDye800 are shown. Phosphate-buffered saline (pH = 7.4) was used as vehicle. Animal were monitored at specific time points over the course of 15 days after peptide administration. For necropsy, 3 animals/sex/group were euthanized on days 2 and 15. NAD – No abnormalities detected.

Chen J, *et al. Gut* 2021; 70:1010–1013. doi: 10.1136/gutjnl-2020-322945

Supplementary Table 7 – In vivo imaging results

Methods	Accuracy	AUC
T/B ratio from QRH*-Cy5	86%	0.95
T/B ratio from KSP*-IRDye800	82%	0.94
Maximum T/B ratio	86%	0.96
Support vector machine (SVM)	91%	0.97
Logistic regression	91%	0.97

Notes: Classification accuracy for in vivo images versus highest grade of pathology is shown for different methods using leave-one-out cross-validation (LOOCV). Average AUC with 1000 bootstrap samples using the models trained on all of the data is shown. SVM and logistic regression models combine T/B ratios from QRH*-Cy5 and KSP*-IRDye800.

Chen J, *et al. Gut* 2021; 70:1010–1013. doi: 10.1136/gutjnl-2020-322945

Supplementary figures

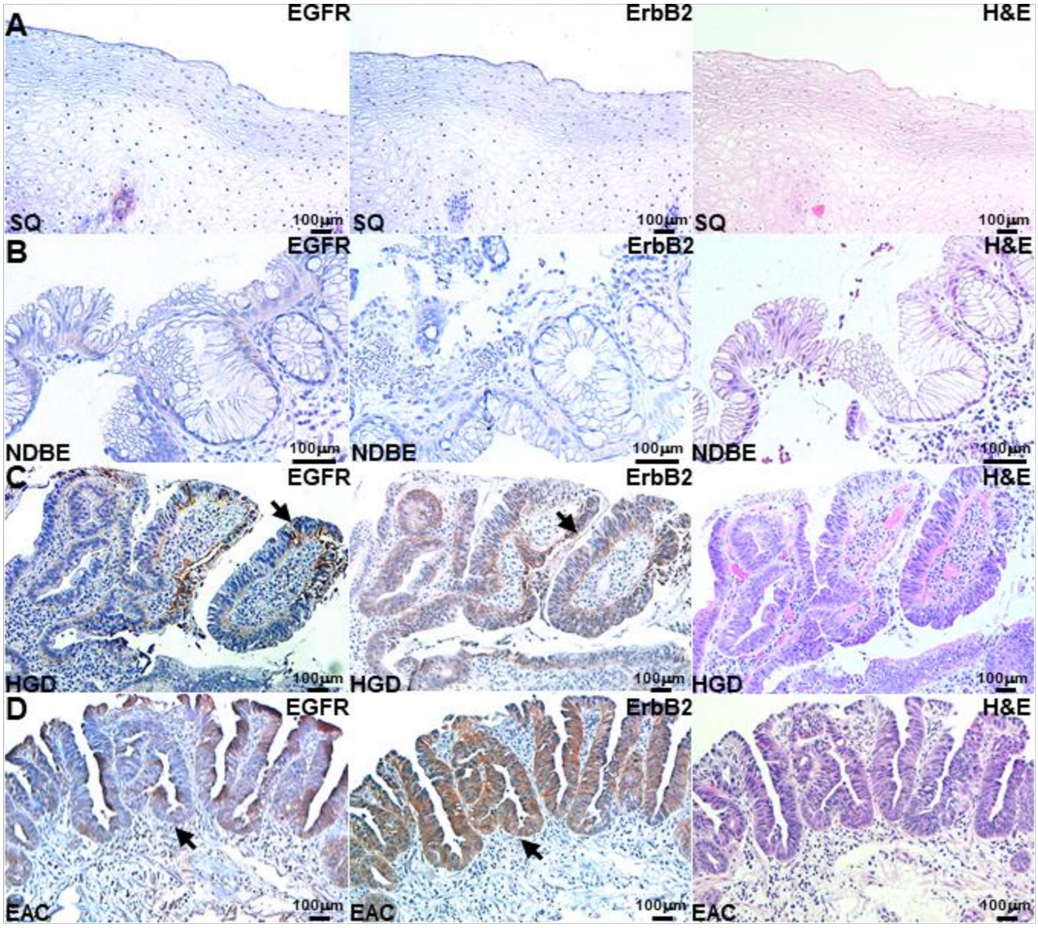

Fig. **S1** – **Immunohistochemistry**. Minimal staining is seen with anti-EGFR and anti-ErbB2 to **A**) SQ and **B**) NDBE, while strong staining is seen to the cell surface (arrow) for **C**) HGD and **D**) EAC. Representative histology (H&E) is shown.

Chen J, *et al. Gut* 2021; 70:1010–1013. doi: 10.1136/gutjnl-2020-322945

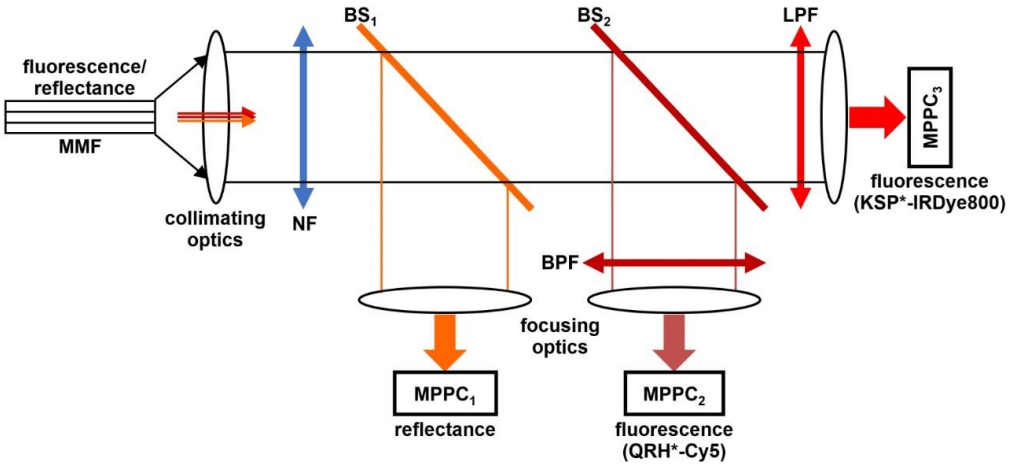

Fig. **S2** – **Detection scheme**. Fluorescence and reflectance are collected and delivered by multi-mode fibers (MMF). A notch filter (NF) attenuates the excitation beam at $\lambda = 785$ nm. Reflectance is deflected by a beam splitter BS_1 with center wavelength at $\lambda = 647$ nm, and detected by a multi-pixel photon counter ($MPPC_1$). Fluorescence from QRH*-Cy5 is deflected by a dichroic beam splitter (BS_2) centered at $\lambda = 785$ nm. A bandpass filter (BPF) transmits fluorescence between 668-726 nm for detection by $MPPC_2$. Fluorescence from KSP*-IRDye800 passes through BS_2 and a long pass filter (LPF) with cutoff at $\lambda = 805$ nm for detection by $MPPC_3$.

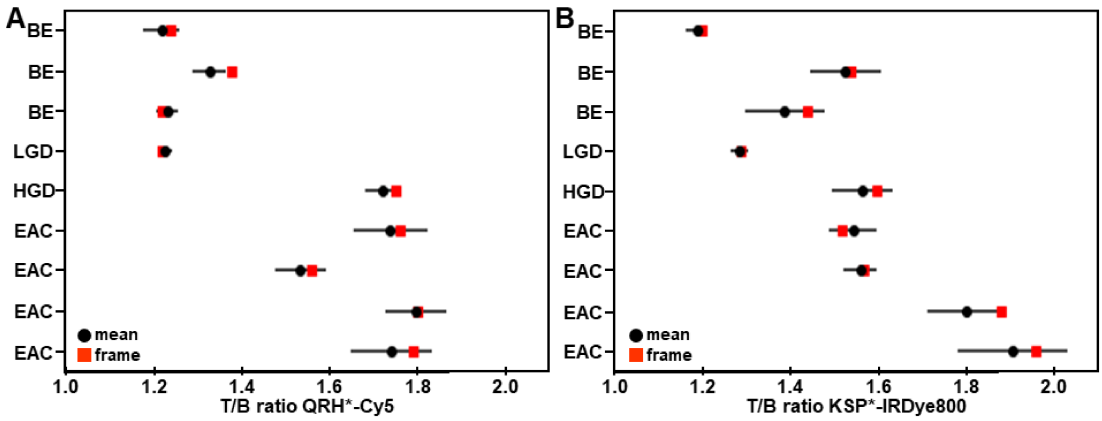

Fig. **S3 – T/B variability within video segment**. Multiple individual frames were extracted from representative video streams collected in vivo from the esophagus for expression of **A**) EGFR and **B**) ErbB2. The mean (circle) and standard deviation of replicate estimated T/B ratios are shown in black. The square (red) shows the value for the representative frame. For EGFR, the average coefficient of variation (CV), defined as the standard deviation divided by the mean, was 3.2%. The representative images had a 1.2% higher T/B ratio than the average of the replicates, $P = 0.03$ by paired t-test of log-transformed values. Bias was 0.78% higher in the HGD/EAC samples, 1.6% versus 0.8%, $P = 0.45$ by two-sample t-test of the differences of log-transformed data. For ErbB2, the average CV was 4.2%. Representative images had a 1.8% higher T/B ratio than the average of the replicates, $P = 0.015$. Bias was 0.02% lower in the HGD/EAC samples (1.7% versus 1.9%, $P = 0.90$).

Supplementary videos

Video S1 – Peptides are topically administered to the distal esophagus via a standard spray catheter.

Video S2 – After 5 minutes for incubation, unbound peptides are washed away with tap water using an endoscopic irrigator.

Video S3 – The mmSFE is passed through the working channel of the endoscope into the esophageal lumen to collect fluorescence and reflectance images

Video S4 – Real-time white light video of SQ.

Video S5 – Real-time fluorescence video of EGFR expression from SQ.

Video S6 – Real-time fluorescence video of ErbB2 expression from SQ.

Video S7 – Real-time reflectance video from SQ.

Video S8 – Real-time merged video from SQ.

Video S9 – Real-time white light video of NDBE.

Video S10 – Real-time fluorescence video of EGFR expression from NDBE.

Video S11 – Real-time fluorescence video of ErbB2 expression from NDBE.

Video S12 – Real-time reflectance video from NDBE.

Video S13 – Real-time merged video from NDBE.

Video S14 – Real-time white light video of HGD.

Video S15 – Real-time fluorescence video of EGFR expression from HGD.

Video S16 – Real-time fluorescence video of ErbB2 expression from HGD.

Video S17 – Real-time reflectance video from HGD.

Video S18 – Real-time merged video from HGD.

Video S19 – Real-time white light video of EAC.

Video S20 – Real-time fluorescence video of EGFR expression from EAC.

Video S21 – Real-time fluorescence video of ErbB2 expression from EAC.

Video S22 – Real-time reflectance video from EAC.

Video S23 – Real-time merged video from EAC.

Chen J, *et al. Gut* 2021; 70:1010–1013. doi: 10.1136/gutjnl-2020-322945